

Drift-Based Policy Optimization: Native One-Step Policy Learning for Online Robot Control

Yuxuan Gao^{1*}, Yedong Shen^{2*}, Shiqi Zhang³, Wenhao Yu¹, Yifan Duan², Jia pan⁴, Jiajia Wu⁴,
Jiajun Deng^{5,†}, Yanyong Zhang^{3,†} *Fellow, IEEE*

Abstract—Although multi-step generative policies achieve strong performance in robotic manipulation by modeling multimodal action distributions, they require multi-step iterative denoising at inference time. Each action therefore needs tens to hundreds of network function evaluations (NFEs), making them costly for high-frequency closed-loop control and online reinforcement learning (RL). To address this limitation, we propose a two-stage framework for native one-step generative policies that shifts refinement from inference to training. First, we introduce the Drift-Based Policy (DBP), which leverages fixed-point drifting objectives to internalize iterative refinement into the model parameters, yielding a one-step generative backbone by design while preserving multimodal action modeling capacity. Second, we develop Drift-Based Policy Optimization (DBPO), an online RL framework that equips the pretrained backbone with a compatible stochastic interface, enabling stable on-policy updates without sacrificing the one-step deployment property. Extensive experiments demonstrate the effectiveness of the proposed framework across offline imitation learning, online fine-tuning, and real-world control scenarios. DBP matches or exceeds the performance of multi-step diffusion policies while achieving up to 100× faster inference. It also consistently outperforms existing one-step baselines on challenging manipulation benchmarks. Moreover, DBPO enables effective and stable policy improvement in online settings. Experiments on a real-world dual-arm robot demonstrate reliable high-frequency control at 105.2, Hz. Code will be available at <https://github.com/YuxuanGao0822/DBPO>.

Index Terms—Visuomotor Control, Generative Policies, Multimodal Learning, Online Reinforcement Learning

I. INTRODUCTION

Robotic manipulation requires policies capable of executing complex visuomotor tasks across diverse conditions. A primary challenge arises from action multimodality: for a given observation, multiple valid action sequences can exist due to task ambiguity, demonstration diversity, or environmental stochasticity. This challenge has motivated recent research toward expressive generative policies that model actions as conditional distributions rather than deterministic mappings.

Multi-step generative policies, exemplified by the Diffusion Policy [1] and DP3 [2], demonstrate strong performance on challenging manipulation tasks through iterative refinement during inference. However, this iterative mechanism necessitates multiple network evaluations per action—often tens to hundreds of denoising or transport steps—which incurs substantial inference latency. This latency proves prohibitive for high-frequency closed-loop control and severely restricts online reinforcement learning [3]–[5].

To address this bottleneck, recent studies explore one-step or few-step generative policies, with the goal of reducing the process of robotic control to a single network function evaluation. These approaches typically fall into two categories. Methods based on diffusion acceleration [6]–[10] obtain one-step behavior by distilling, compressing, or accelerating pretrained multi-step generators in a consistency style, thereby inheriting the capabilities of the teacher model while retaining a dependency on multi-step pretraining. Mean-flow-based policies [11]–[14] achieve one-step deployment without distillation, yet they rely on auxiliary quality-preserving or corrective mechanisms—such as dispersive losses, directional alignment, or instantaneous-velocity constraints—to maintain performance under strict 1-NFE constraints.

Although both categories demonstrate the practical utility of efficient inference, each entails a distinct trade-off. Distillation-based routes leverage robust teacher models but remain tied to multi-step pretraining, whereas correction-based routes stabilize strict 1-NFE generation through additional objective terms, often introducing extra optimization constraints. In this work, the term native one-step refers to formulations in which 1-NFE inference arises directly from the training objective itself, rather than from post-hoc acceleration or objective coupling. This distinction reveals a remaining gap in current policy learning: a formulation that jointly delivers high policy quality and one-step efficiency as an intrinsic property of the backbone. Addressing this gap requires rethinking policy learning from a training-centric perspective, where efficiency and performance are co-designed rather than sequentially approximated.

We address this gap by building upon Drifting Models [15], a generative principle designed to be one-step by construction. Unlike diffusion and flow methods that perform iterative refinement during inference, drifting shifts the refinement process entirely to the training phase. During the learning phase, the generator progressively internalizes corrective behaviors through the training-time evolution of the pushforward distribution, such that post-training inference requires only a single forward pass to produce high-quality samples. Mechanistically,

* These authors contributed equally.

† Corresponding author

¹Institute of Advanced Technology, University of Science and Technology of China, Hefei 230026, China {yuxuangao, wenhaoyu}@mail.ustc.edu.cn

²School of Computer Science and Technology, University of Science and Technology of China, Hefei 230026, China {sydong2002, dyf0202}@mail.ustc.edu.cn

³School of Artificial Intelligence and Data Science, University of Science and Technology of China, Hefei 230026, China {zhangshiqi_1127, yanyongz}@mail.ustc.edu.cn

⁴iflytek, Hefei 230088, China {jiapan, jiajiawu}@iflytek.com

⁵School of information Science and Technology, University of Science and Technology of China, Hefei 230026, China dengjj@ustc.edu.cn

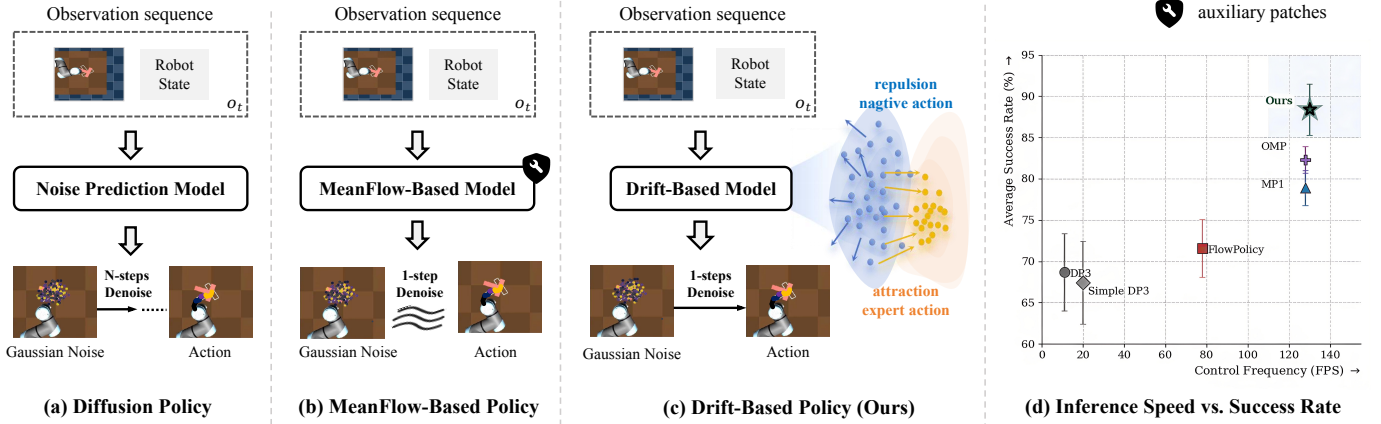


Fig. 1: Generative policy paradigms for robot control. (a) Multi-step diffusion policies rely on iterative denoising at inference. (b) One-step mean-flow policies generate actions in one pass with auxiliary corrections. (c) Drift-Based Policy internalizes attraction-repulsion refinement during training, yielding a native one-step generator. (d) Our method achieves the best average success rate and control frequency on Adroit and MetaWorld against established generative baselines.

this design differs from post-hoc acceleration: low-latency deployment is achieved through training dynamics rather than through compression or distillation. For robotic control, this distinction proves practically significant because latency is guaranteed by the formulation of the policy itself, yielding a predictable 1-NFE deployment path without reliance on additional corrective modules.

This principle is instantiated as the Drift-Based Policy (DBP), a native 1-NFE policy backbone for observation-conditioned action generation in robotic manipulation. The DBP is designed around three practical requirements for deployment-oriented policy learning. First, it utilizes a drifting formulation specialized for sequential action-chunk prediction under observation conditioning. Second, it provides native support for heterogeneous sensory modalities, including low-dimensional states, RGB images, 3D point clouds, and multi-camera inputs. Third, it strictly preserves 1-NFE inference under closed-loop control. This design establishes drifting as a practical native one-step policy backbone that achieves high performance through native generative principles rather than through post-hoc compression of multi-step models.

However, a robust one-step backbone alone remains insufficient for a complete control framework. As an offline imitation learner, the DBP primarily reproduces the demonstration distribution and can be limited when the improvement of returns requires behavior beyond demonstration support. Online RL provides complementary benefits by directly optimizing task rewards, improving recovery from off-demonstration states, and expanding effective state-space coverage in evaluation settings. To bridge this gap, we introduce Drift-Based Policy Optimization (DBPO), which extends the DBP to online reinforcement learning while preserving the 1-NFE deployment efficiency of the backbone. The primary challenge involves concurrently preserving the multimodal expressiveness of the pretrained one-step generator, supporting exact action-likelihood evaluation for standard on-policy optimization algorithms, and maintaining strict 1-NFE inference during deploy-

ment. This challenge is addressed through a minimal stochastic interface that enables exact likelihood computation for on-policy updates while keeping the deterministic generation path unchanged during deployment. Consequently, DBPO performs on-policy RL updates without sacrificing the native one-step property established during offline training.

The proposed framework is evaluated along two complementary axes. First, the DBP is compared against the multi-step Diffusion Policy to verify that native one-step generation can match or exceed multi-step performance at a fraction of the inference cost. Across the simulation suite of the Diffusion Policy (12 tasks), the DBP improves the family-level average score from 0.79 to 0.83 while reducing the inference cost from 100 NFEs to 1. Second, the proposed framework is benchmarked against competitive 1-NFE baselines across both offline imitation learning and online fine-tuning settings. For point-cloud manipulation across Adroit and Meta-World, the DBP establishes a state-of-the-art success rate of 88.4%, consistently outperforming representative 1-NFE baselines. The comprehensive evaluation further includes online RL benchmarks on RoboMimic and D4RL, where DBPO improves upon a strong one-step offline initialization via PPO fine-tuning while strictly preserving 1-NFE deployment. Additionally, real-world deployment on a physical dual-arm UR5 setup yields a 75% success rate at 105.2 Hz, confirming its practical feasibility for high-frequency control.

The contributions of this work are summarized as follows:

- We introduce the Drift-Based Policy (DBP), a native one-step generative policy for robotic control. This approach shifts iterative refinement from inference to training via fixed-point drifting objectives, achieving a 1-NFE deployment by design while preserving the capacity for multimodal action modeling.
- We propose Drift-Based Policy Optimization (DBPO), an online reinforcement learning framework built upon DBP. This framework overcomes the performance ceiling and spatial generalization limits of offline imitation learning

by enabling exact-likelihood on-policy updates while preserving a deterministic one-step deployment path.

- We present comprehensive empirical validation across simulation, real-world deployment, and both offline and online learning regimes. The results demonstrate that DBP achieves competitive or superior performance compared to multi-step diffusion-based policies while reducing inference to a single forward pass, and consistently outperforms existing 1-NFE baselines. Furthermore, DBPO enables stable and effective policy improvement in online settings, and supports high-frequency real-world control.

II. RELATED WORK

A. Diffusion-Based Visuomotor Policies and One-Step Acceleration

Diffusion models have emerged as a central paradigm in robotic policy learning, as iterative denoising provides a flexible mechanism to represent multimodal action distributions. Diffusion Policy [1] formulates imitation learning as conditional denoising over action chunks, while DP3 [2] extends this formulation to 3D point-cloud observations. Subsequent variants enhance policy quality through architectural innovations and inductive-bias designs tailored for visuomotor control. A common limitation of this family of methods resides in deployment latency: each control query necessitates repeated denoising updates, thereby increasing closed-loop response times and interaction costs in online learning.

To mitigate these computational costs, recent studies investigate one-step acceleration via distillation and consistency-style objectives [6]–[10], [16]–[19]. These approaches can inherit robust behaviors from pretrained multi-step teacher models; however, the 1-NFE capability of these methods is typically acquired through compression pipelines or auxiliary acceleration stages. Consequently, one-step behavior frequently emerges as a result of post-hoc transformations rather than as an intrinsic property of the base policy objective.

B. Flow-Style and Mean-Flow-Based One-Step Policy Learning

In parallel, another prominent research direction pursues one-step generation via flow matching, consistency-style flow training, and mean-flow reformulations [20]–[25]. FlowPolicy, AdaFlow, and ManiFlow adapt flow-style policies for application in robotic manipulation [26]–[30]. Recent mean-flow-based methods, including MP1 [11], DM1 [12], OMP [31], and MVP [13], demonstrate strong 1-NFE performance across challenging benchmarks [14], [32], [33].

In contrast to diffusion acceleration, these approaches avoid explicit teacher distillation and optimize one-step behavior in a more direct manner. However, they commonly rely on carefully designed auxiliary constraints—such as dispersive regularization, directional alignment, or instantaneous-velocity consistency—to stabilize the optimization process under strict one-step inference [34]. This line of research demonstrates the practical feasibility of 1-NFE control, while simultaneously highlighting that the preservation of policy quality frequently

depends on additional corrective objectives beyond the core generative mapping.

C. Online RL for Generative Policies

Recent studies further integrate online RL into generative policy backbones to elevate performance beyond the limits of offline imitation. DPPO [3] integrates PPO into multi-step diffusion policies, whereas ReinFlow [4], DMPO [5], and MVP [13] extend one-step flow and mean-flow frameworks via online optimization [35]–[38]. Related efforts in domain-general generative RL similarly demonstrate that interaction-driven learning can enhance returns and robustness compared to static behavior cloning.

These advancements underscore a central trade-off in the online optimization of generative control: methods must achieve reward-driven adaptation from interaction while preserving deployment efficiency and policy stability under standard on-policy updates. The proposed method targets this regime by retaining strict 1-NFE execution and providing a compatible online optimization path.

III. PRELIMINARIES

This section briefly reviews the principle of Drifting Models (DM) [15]. DM formulates generation as the training-time evolution of pushforward distributions; consequently, corrective dynamics are absorbed during optimization, and inference remains strictly one-step.

Let $\mathbf{z} \sim p_0 = \mathcal{N}(\mathbf{0}, \mathbf{I}_C)$ and let $f_\theta : \mathbb{R}^C \rightarrow \mathbb{R}^D$ denote a generator. A generated sample and its induced distribution are defined as:

$$\mathbf{x} = f_\theta(\mathbf{z}), \quad q_\theta = [f_\theta]_{\#} p_0. \quad (1)$$

Here, C and D represent the latent and output dimensions, respectively, while $[f_\theta]_{\#} p_0$ denotes the pushforward of p_0 through f_θ .

Let p denote the target distribution on \mathbb{R}^D . During optimization, the parameters θ_k at iteration k induce the sequence $q_k = [f_{\theta_k}]_{\#} p_0$. For a fixed latent seed, the sample $\mathbf{x}_k = f_{\theta_k}(\mathbf{z})$ evolves according to

$$\mathbf{x}_{k+1} = \mathbf{x}_k + \mathcal{V}_{p, q_k}(\mathbf{x}_k), \quad (2)$$

where $\mathcal{V}_{p, q}(\mathbf{x}) \in \mathbb{R}^D$ denotes a drifting field. DM adopts an anti-symmetric construction, $\mathcal{V}_{p, q}(\mathbf{x}) = -\mathcal{V}_{q, p}(\mathbf{x})$, which implies that $\mathcal{V}_{p, p}(\mathbf{x}) = \mathbf{0}$, thereby ensuring zero drift at distributional equilibrium. This property motivates the formulation of a fixed-point target:

$$\tilde{\mathbf{x}} = \text{sg}(f_\theta(\mathbf{z}) + \mathcal{V}_{p, q_\theta}(f_\theta(\mathbf{z}))), \quad (3)$$

where $\text{sg}(\cdot)$ represents the stop-gradient operation and $\tilde{\mathbf{x}}$ signifies the frozen drifted target. The corresponding training objective is given by

$$\mathcal{L}_{\text{DM}} = \mathbb{E}_{\mathbf{z} \sim p_0} \left[\|f_\theta(\mathbf{z}) - \tilde{\mathbf{x}}\|_2^2 \right]. \quad (4)$$

Minimizing Eq. (4) regresses the current predictions toward the drifted targets; consequently, field corrections are progressively encoded within the network parameters. To obtain

a computable field, DM employs a kernelized interaction formulation:

$$\mathcal{V}_{p,q}(\mathbf{x}) = \mathbb{E}_{\mathbf{y}^+ \sim p, \mathbf{y}^- \sim q} [\mathcal{K}(\mathbf{x}, \mathbf{y}^+, \mathbf{y}^-)], \quad (5)$$

Here, \mathbf{y}^+ and \mathbf{y}^- represent positive and negative samples drawn from p and q , respectively, and $\mathcal{K} : \mathbb{R}^D \times \mathbb{R}^D \times \mathbb{R}^D \rightarrow \mathbb{R}^D$ constitutes an interaction kernel. In practice, this formulation yields an attraction toward target samples and a repulsion from model samples, while simultaneously preserving anti-symmetry.

In the proposed policy setting, generated samples correspond to action chunks, and the generator operates under observation conditioning. Section IV specializes this generic drifting objective for one-step robotic control and the online RL extension thereof.

IV. METHOD

This section introduces a two-stage framework that preserves single-pass deployment while enabling online policy improvement. Stage 1, DBP, learns a native one-step generative policy from offline demonstrations. Stage 2, DBPO, adds an exact-likelihood stochastic adapter for PPO-style updates while keeping strict 1-NFE execution. Figure 2 summarizes the pipeline. Additional method details are provided in the Supplementary Material.

Throughout this section, bold symbols denote vectors, matrices, or tensors. The index t denotes environment step, i minibatch sample, r generated hypothesis index for a fixed observation, h step index within an action chunk, m scalar coordinate in \mathbb{R}^{d_a} , and d flattened coordinate in \mathbb{R}^S .

A. Policy Setup

At environment step t , let $\mathbf{o}_t^{\text{hist}} := \mathbf{o}_{t-T_o+1:t}$ denote the observation history of length T_o . The policy predicts an action chunk of horizon H in a single forward pass:

$$\mathbf{x}_t := [\mathbf{a}_t^1, \dots, \mathbf{a}_t^H] \in \mathbb{R}^D, \quad \mathbf{a}_t^h \in \mathbb{R}^{d_a}, \quad D = Hd_a, \quad (6)$$

Here, \mathbf{x}_t is the predicted chunk, \mathbf{a}_t^h is the h -th action, d_a is the per-step action dimension, and D is the flattened chunk dimension. Given an offline demonstration dataset $\mathcal{D} = \{(\mathbf{o}_i^{\text{hist}}, \mathbf{x}_i^E)\}_{i=1}^N$, where each pair contains an observation history and the aligned expert action chunk thereof, with $\mathbf{x}_i^E = [\mathbf{a}_i^{E,1}, \dots, \mathbf{a}_i^{E,H}]$, we use a one-step conditional generator with latent prior $\mathbf{z}_t \sim p_0 = \mathcal{N}(\mathbf{0}, \mathbf{I})$ and fixed generation index $\tau = 0$:

$$\begin{aligned} \hat{\mathbf{x}}_t &= f_\theta(\mathbf{o}_t^{\text{hist}}, \mathbf{z}_t; \tau = 0), \\ q_\theta(\cdot | \mathbf{o}_t^{\text{hist}}) &= [f_\theta(\mathbf{o}_t^{\text{hist}}, \cdot; \tau = 0)]_{\#} p_0, \end{aligned} \quad (7)$$

Here, f_θ is the one-step generator, $\hat{\mathbf{x}}_t$ is the generated chunk, and $q_\theta(\cdot | \mathbf{o}_t^{\text{hist}})$ is the induced conditional action distribution. During deployment, receding-horizon control executes the sub-window starting at chunk index T_o with an execution length H_e : $\mathbf{x}_t^{\text{exec}} = [\mathbf{a}_t^{T_o}, \dots, \mathbf{a}_t^{T_o+H_e-1}]$. The boundary conditions $1 \leq T_o \leq H$ and $1 \leq H_e \leq H - T_o + 1$ are strictly required to ensure the mathematical validity of the executed action slice.

B. Drift-Based Policy Learning

DBP trains f_θ by shaping a drift field in action space. Multiple hypotheses interact with expert anchors so that updates combine attraction to expert behavior and repulsion among hypotheses. The corrective dynamics are absorbed in training; deployment remains one-step. For a trajectory minibatch $\{(\mathbf{o}_i^{\text{hist}}, \mathbf{x}_i^E)\}_{i=1}^B$, we draw G latent samples per observation and generate hypotheses $\hat{\mathbf{x}}_i^{(r)} = f_\theta(\mathbf{o}_i^{\text{hist}}, \mathbf{z}_i^{(r)}; \tau = 0)$, $r \in \{1, \dots, G\}$. Here, G controls the number of hypotheses per observation. During deployment, a single latent code is sampled and $f_\theta(\mathbf{o}_t^{\text{hist}}, \mathbf{z}_t; \tau = 0)$ is evaluated once, precluding iterative refinement.

Drifting Objective in Action Space. Two training views are used. In chunk mode, trajectories are flattened with $S = Hd_a$ and drifting is applied once per sample. In step-wise mode, the same objective is applied to each step slice with $S = d_a$ and then averaged over H steps. For each minibatch, let $\mathbf{G} \in \mathbb{R}^{B \times G \times S}$ represent the generated hypotheses, let $\bar{\mathbf{G}} = \text{sg}(\mathbf{G})$ be the detached copy thereof, and let $\mathbf{Y} = [\bar{\mathbf{G}}, \mathbf{N}^-, \mathbf{P}^+]$ denote the reference pool composed of generated references, optional negatives, and expert positives. Let $C_n = |\mathbf{N}^-|$, $C_p = |\mathbf{P}^+|$, and $U = G + C_n + C_p$. The negative-reference indices are denoted by $\mathcal{I}^- = \{1, \dots, G + C_n\}$, and the positive-reference indices are denoted by $\mathcal{I}^+ = \{G + C_n + 1, \dots, U\}$. Omitting implementation constants, the core geometry is defined by

$$\begin{aligned} d_{i,r,u} &:= \|\bar{\mathbf{G}}_{i,r,:} - \mathbf{Y}_{i,u,:}\|_2, \quad s_{\text{norm}} := \mathbb{E}_{i,r,u}[d_{i,r,u}], \\ A_{i,r,u}^{(R)} &:= \text{SymSoftmax}\left(-\frac{d_{i,r,u}}{R s_{\text{norm}}}\right), \quad R \in \mathcal{R}. \end{aligned} \quad (8)$$

Here, $d_{i,r,u}$ is the spatial pairwise distance, s_{norm} is the mean distance, and $A_{i,r,u}^{(R)}$ is the symmetric affinity at scale R . The set \mathcal{R} contains finitely many interaction scales. A numerical floor is applied to ensure stability by $s_{\text{norm}} > 0$.

Define side masses $S_{i,r,-}^{(R)} := \sum_{u \in \mathcal{I}^-} A_{i,r,u}^{(R)}$ and $S_{i,r,+}^{(R)} := \sum_{u \in \mathcal{I}^+} A_{i,r,u}^{(R)}$. The balanced coefficients are formulated as

$$\alpha_{i,r,u}^{(R)} = \begin{cases} -A_{i,r,u}^{(R)} S_{i,r,+}^{(R)}, & u \in \mathcal{I}^-, \\ A_{i,r,u}^{(R)} S_{i,r,-}^{(R)}, & u \in \mathcal{I}^+. \end{cases} \quad (9)$$

This formulation yields repulsion from \mathcal{I}^- and attraction toward \mathcal{I}^+ with cross-side mass balancing. In particular, $\sum_{u \in \mathcal{I}^-} \alpha_{i,r,u}^{(R)} = -\sum_{u \in \mathcal{I}^+} \alpha_{i,r,u}^{(R)}$, which enforces antisymmetric mass exchange between the two sides.

For each scale R , the drift contribution is $\mathbf{F}_{i,r}^{(R)} := \sum_{u=1}^U \alpha_{i,r,u}^{(R)} (\mathbf{Y}_{i,u,:} - \bar{\mathbf{G}}_{i,r,:}) / s_{\text{norm}}$. After per-scale RMS normalization and aggregation, $\mathbf{V}_{i,r,:} := \sum_{R \in \mathcal{R}} \hat{\mathbf{F}}_{i,r,:}^{(R)}$. The fixed-point regression form is

$$\begin{aligned} \tilde{\mathbf{X}} &= \text{sg}(\bar{\mathbf{G}}/s_{\text{norm}} + \mathbf{V}), \\ \ell_i &= \frac{1}{GS} \sum_{r=1}^G \sum_{d=1}^S \left(\frac{G_{i,r,d}}{s_{\text{norm}}} - \tilde{X}_{i,r,d} \right)^2, \end{aligned} \quad (10)$$

where $\text{sg}(\cdot)$ is stop-gradient and \mathbf{V} is the aggregated multi-scale drift. The final DBP objective constitutes the sample

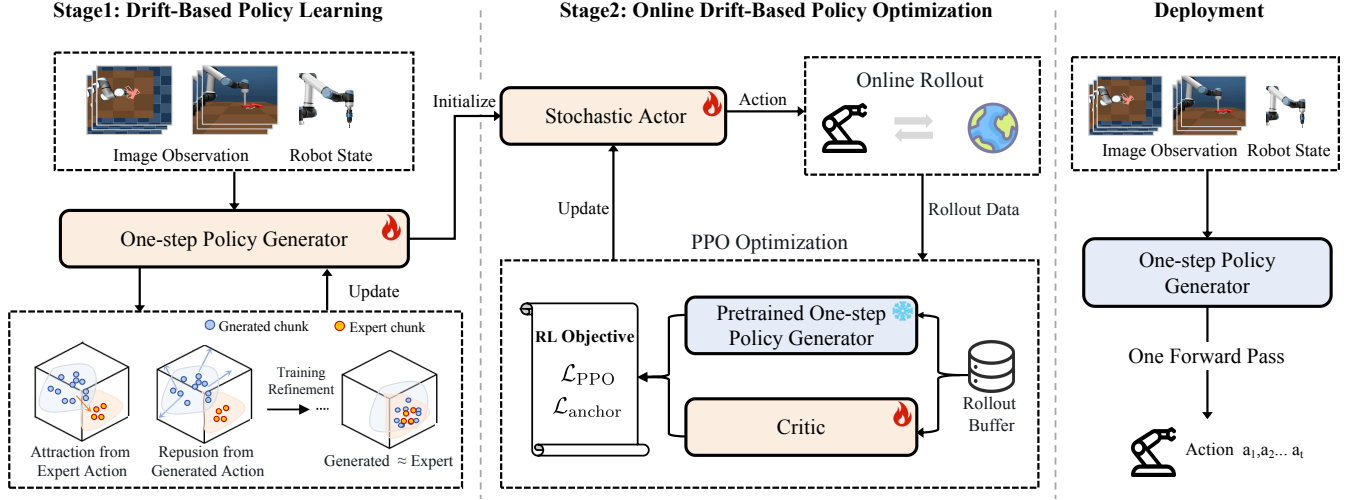


Fig. 2: Two-stage Drift-Based Policy framework. Stage 1 learns a native one-step generator offline via attraction-repulsion refinement during training. Stage 2 fine-tunes a stochastic actor initialized from the pretrained backbone with on-policy PPO and anchor regularization, while deployment remains one-step (1-NFE).

average in chunk mode and the time-averaged sample loss in step-wise mode:

$$\mathcal{L}_{\text{DBP}} = \begin{cases} \frac{1}{B} \sum_{i=1}^B \ell_i, & \text{chunk mode,} \\ \frac{1}{BH} \sum_{h=1}^H \sum_{i=1}^B \ell_i^{(h)}, & \text{step-wise mode,} \end{cases} \quad (11)$$

where $\ell_i^{(h)}$ is the sample loss on the h -th action slice with $S = d_a$. Detailed pseudocode, numerical stabilizers, and additional derivations are provided in the Supplementary Material for readability.

Principled Divergence View and Convergence Guarantee.

From Eq. (10), the chunk-mode objective equals the mean squared drift magnitude, $\mathcal{L}_{\text{DBP}} = \mathcal{D}_{\text{drift}}(q_\theta, p; \mathcal{R})$, because $\bar{\mathbf{G}} = \text{sg}(\mathbf{G})$ keeps forward values unchanged while blocking gradients in target construction. Here, p is the expert conditional action distribution and q_θ is the generated conditional distribution.

Under standard stochastic approximation assumptions (smooth $\mathcal{D}_{\text{drift}}$, unbiased bounded-variance minibatch gradients, and Robbins–Monro step sizes $\sum_k \eta_k = \infty$, $\sum_k \eta_k^2 < \infty$), SGD on Eq. (11) reaches a first-order stationary regime, i.e., $\liminf_{k \rightarrow \infty} \mathbb{E}[\|\nabla_{\theta} \mathcal{D}_{\text{drift}}(\theta_k)\|_2^2] = 0$. If, additionally, the generator Jacobian is locally full-rank on the support of p_0 and the drifting field is identifiable at equilibrium (i.e., $\mathcal{V}_{p,q}(\mathbf{x}) \equiv \mathbf{0} \Rightarrow q = p$), zero-drift stable points correspond to the target distribution in the induced action space. This identifiability statement is used as an additional sufficient assumption.

Numerical stabilizers (e.g., clipping, masking constants, and finite-precision safeguards) constitute implementation details and do not alter the aforementioned optimization principle.

C. Online Drift-Based Policy Optimization

Although DBP provides a robust one-step offline initialization, offline imitation alone is insufficient to address reward-driven distribution shifts encountered during online interaction. The extension of DBP to online RL must concurrently

satisfy three requirements: preserving the pretrained one-step generator, providing exact likelihoods for standard PPO [39], and maintaining deployment at 1-NFE. DBPO fulfills these requirements via a minimal stochastic adapter constructed upon the pretrained backbone.

For brevity within this subsection, let $\mathbf{o}_t := \mathbf{o}_t^{\text{hist}}$. In Eq. (7), the marginal $q_\theta(\cdot | \mathbf{o}_t)$ is implicit because it integrates over latent variables, whereas PPO requires explicit rollout likelihoods. DBPO therefore uses a trainable active backbone, a frozen reference backbone, and an analytic stochastic actor $\pi_{\theta, \psi}$.

Exact-Likelihood Stochastic Actor. For generic inputs (\mathbf{o}, \mathbf{z}) , the active backbone predicts the latent-conditioned chunk mean $\mu_\theta(\mathbf{o}, \mathbf{z})$ and an observation feature representation $\mathbf{c}_\theta(\mathbf{o})$. A diagonal log-standard-deviation head is attached as $\log \sigma_\psi(\mathbf{o}) := g_\psi(\mathbf{c}_\theta(\mathbf{o}))$, with $\log \sigma_\psi(\mathbf{o}) \in \mathbb{R}^D$ spanning the action dimension.

The resulting actor is defined as:

$$\pi_{\theta, \psi}(\mathbf{x} | \mathbf{o}, \mathbf{z}) = \mathcal{N}(\mathbf{x}; \mu_\theta(\mathbf{o}, \mathbf{z}), \text{diag}(\sigma_\psi(\mathbf{o})^2)). \quad (12)$$

Here, $\sigma_\psi(\mathbf{o})$ controls exploration noise. During rollout, the policy samples $\mathbf{z}_t \sim p_0$ and then $\mathbf{x}_t \sim \pi_{\theta, \psi}(\cdot | \mathbf{o}_t, \mathbf{z}_t)$, and stores $(\mathbf{z}_t, \mathbf{x}_t)$ in the buffer. Because PPO reuses the same stored latent \mathbf{z}_t in evaluation epochs, Eq. (12) provides exact conditional rollout likelihoods.

Executed-Prefix Likelihood. Online updates are restricted to the executed prefix $\mathbf{x}_t^{\text{exec}} = [\mathbf{a}_t^{T_o}, \dots, \mathbf{a}_t^{T_o+H_e-1}]$. Its conditional log-likelihood is

$$\log \pi_{\theta, \psi}(\mathbf{x}_t^{\text{exec}} | \mathbf{o}_t, \mathbf{z}_t) = \sum_{h=T_o}^{T_o+H_e-1} \sum_{m=1}^{d_a} \log \mathcal{N}(a_{t,m}^h, \mu_{\theta,m}^h(\mathbf{o}_t, \mathbf{z}_t), \sigma_{\psi,m}^h(\mathbf{o}_t)^2). \quad (13)$$

Here, $h \in \{T_o, \dots, T_o + H_e - 1\}$ indexes executed steps and $m \in \{1, \dots, d_a\}$ indexes scalar action coordinates. The terms $\mu_{\theta,m}^h(\mathbf{o}_t, \mathbf{z}_t)$ and $\sigma_{\psi,m}^h(\mathbf{o}_t)$ are scalar components of the actor mean and standard deviation in Eq. (12). Under closed-loop

re-planning, unexecuted suffix actions are replaced at the next environment step and therefore do not enter current-step credit assignment. Consequently, optimizing only the executed prefix remains consistent with on-policy rollouts used to estimate \hat{A}_t .

Joint-Policy View and Ratio Equivalence. Define the joint policy as $\tilde{\pi}_{\theta,\psi}(\mathbf{x}^{\text{exec}}, \mathbf{z} \mid \mathbf{o}) := p_0(\mathbf{z}) \pi_{\theta,\psi}(\mathbf{x}^{\text{exec}} \mid \mathbf{o}, \mathbf{z})$. Here, $p_0(\mathbf{z})$ is fixed and independent of (θ, ψ) . Using the same stored latent \mathbf{z}_t for new and old policies, the PPO importance ratio becomes

$$\tilde{r}_t(\theta, \psi) := \frac{\tilde{\pi}_{\theta,\psi}(\mathbf{x}_t^{\text{exec}}, \mathbf{z}_t \mid \mathbf{o}_t)}{\tilde{\pi}_k(\mathbf{x}_t^{\text{exec}}, \mathbf{z}_t \mid \mathbf{o}_t)} = \frac{\pi_{\theta,\psi}(\mathbf{x}_t^{\text{exec}} \mid \mathbf{o}_t, \mathbf{z}_t)}{\pi_k(\mathbf{x}_t^{\text{exec}} \mid \mathbf{o}_t, \mathbf{z}_t)} =: r_t(\theta, \psi), \quad (14)$$

which demonstrates the exact equivalence between the joint-policy PPO ratio and the conditional ratio employed in DBPO. Consequently, computationally expensive marginalization over the latent variable \mathbf{z} is not required during policy optimization.

PPO Objective with Drift-Based Anchor. Let π_k denote the behavior policy responsible for rollout collection, and let \hat{A}_t denote the advantage estimate. Following standard PPO [39], the importance ratio $r_t(\theta, \psi)$ from Eq. (14) is utilized to represent the PPO objective compactly as

$$\mathcal{L}_{\text{PPO}} = \mathcal{L}_{\text{clip}}(r_t, \hat{A}_t) + c_v \mathcal{L}_{\text{value}} - c_e \mathcal{H}, \quad (15)$$

where $\mathcal{L}_{\text{clip}}$ is the clipped surrogate, $\mathcal{L}_{\text{value}}$ is value regression, \mathcal{H} is the entropy bonus, and $c_v, c_e > 0$ are weights. To reduce drift from the pretrained state θ , we use the anchor loss:

$$\mathcal{L}_{\text{anchor}} = \mathbb{E}_t \left[\left\| \boldsymbol{\mu}_\theta(\mathbf{o}_t, \mathbf{z}_t) - \boldsymbol{\mu}_{\bar{\theta}}(\mathbf{o}_t, \mathbf{z}_t) \right\|_2^2 \right]. \quad (16)$$

This term penalizes the distance between updated and frozen mean predictions under identical latent inputs, which stabilizes policy updates around the pretrained operating region. The complete objective is formulated as:

$$\mathcal{L}_{\text{RL}} = \mathcal{L}_{\text{PPO}} + \lambda_{\text{anchor}} \mathcal{L}_{\text{anchor}}. \quad (17)$$

Here, λ_{anchor} acts as the scalar weight for anchor regularization.

During training, exploration operates via Gaussian noise superimposed on the mean, whereas deployment removes this noise and reverts to the deterministic center. Throughout closed-loop manipulation, the execution of a prediction necessitates exactly one network evaluation, thereby maintaining 1-NFE efficiency.

V. EXPERIMENTS

The experiments evaluate three primary aspects: (1) the capability of the proposed Drift-Based Policy (DBP) to match or exceed the iterative diffusion baseline while reducing inference to exactly 1-NFE; (2) the robustness of the DBP backbone on large-scale 3D point-cloud manipulation benchmarks; and (3) the cross-domain performance gains and real-robot transfer efficacy of its online reinforcement learning extension, Drift-Based Policy Optimization (DBPO).

A. Evaluation Setup and Protocols

Dataset. We evaluate on three benchmark families. (i) In the reproduced Diffusion Policy suite [1], we use Push-T (Image), Push-T (Low-Dim), BlockPush (P1/P2), RoboMimic (Low-Dim), RoboMimic (Image), and Kitchen (12 tasks in total). (ii) For point-cloud one-step evaluation, we follow the MP1/OMP protocol on 37 tasks: 3 Adroit tasks and 34 Meta-World tasks (21 Easy, 4 Medium, 4 Hard, and 5 Very Hard) [11], [31], [40], [41]. (iii) For online RL, we evaluate on 4 RoboMimic manipulation tasks and D4RL locomotion tasks, using the same simplified RoboMimic setting as prior one-step RL baselines [3]–[5], [42], [43].

Metrics. For manipulation tasks, we report success rate; for D4RL locomotion, we report episode return. Computational efficiency is measured by NFE. In the reproduced Diffusion Policy suite, each result is averaged over the last 10 checkpoints, and each checkpoint is averaged over 3 training seeds. In the point-cloud protocol, evaluation is performed every 200 epochs, the top-5 checkpoints per seed are averaged, and mean \pm std across seeds is reported. For online RL benchmarks, each task is evaluated with 100 episodes.

Baselines. We explicitly separate reproduced and quoted baselines. Reproduced baselines include Diffusion Policy in the diffusion suite, and ReinFlow [4] plus DMPO [5] in online RL comparisons. For Adroit/Meta-World point-cloud comparisons, non-ours results are quoted from OMP [31]. Our method follows the same MP1/OMP architecture and training protocol, including the same U-Net backbone, for protocol-matched comparison.

Implementation Details. To isolate algorithmic effects from architectural effects, we match baseline architectures whenever reproduction is performed. In the point-cloud setting, we use the same U-Net backbone and training pipeline as MP1/OMP, without stronger backbones or additional data augmentation. We use 10 demonstrations per task, FPS preprocessing to 512/1024 points, and 84×84 image resizing when applicable. Seeds are $\{0,1,2\}$. Training runs for 3000 epochs on Adroit and 1000 epochs on Meta-World on $8 \times$ NVIDIA RTX 3090 GPUs. Unless otherwise specified, the default temperature set is $\mathcal{R} = \{0.02, 0.05, 0.2\}$. Additional tuning shows task-dependent optima, and task-specific temperature sets are used when dedicated tuning is reported.

B. DBP Compared with Multi-Step Policy

We first test whether DBP preserves policy quality when iterative denoising is replaced by strict 1-NFE inference under the reproduced Diffusion Policy setting.

Table I summarizes the reproduced comparison. DBP increases the task average from 0.79 to 0.83 while reducing inference from 100 NFE to 1 NFE, corresponding to a $100\times$ speedup. At the task level, DBP improves Push-T (Low-Dim), BlockPush, and RoboMimic (Low-Dim), ties Kitchen, and is slightly lower than Diffusion Policy on Push-T (Image) and RoboMimic (Image). In this evaluation setting, these results indicate that drifting can absorb most iterative correction effects into a one-step mapping while retaining substantial efficiency gains.

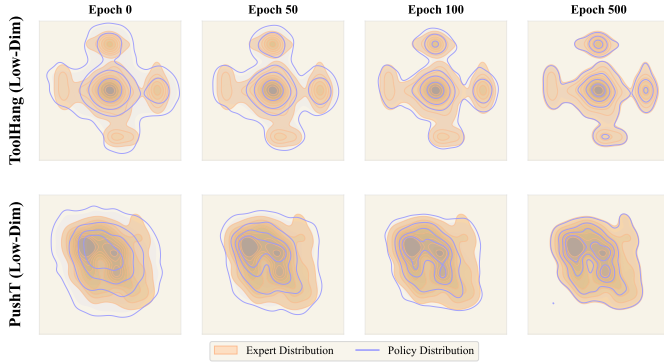


Fig. 3: Evolution of the internalized drift manifold. The policy action distribution (blue) progressively aligns with expert modes (peach) during training.

TABLE I: Comparison between Diffusion Policy and Ours on the Diffusion Policy suite. BlockPush/Kitchen are phase-averaged. Entries report success rate. Best results are in **bold**.

Task	Diffusion Policy (100 NFE)	Ours (1 NFE)
Push-T (Image)	0.91	0.89
Push-T (Low-Dim)	0.85	0.87
BlockPush (P1/P2)	0.24	0.43
RoboMimic (Low-Dim)	0.80	0.92
RoboMimic (Image)	0.91	0.87
Kitchen (P1/P2/P3/P4)	1.00	1.00
Avg.	0.79	0.83

Figure 3 visualizes this transition. Early in training, generated actions are dispersed relative to expert modes; as optimization proceeds, the distribution contracts toward expert-supported regions. This trend is consistent with the drifting hypothesis that corrective dynamics are internalized during training and executed by a single forward pass at deployment.

C. DBP Compared with One-Step Baselines

We evaluate the native one-step quality of DBP before online adaptation, with the goal of isolating the offline backbone under strict 1-NFE inference. Following the MP1/OMP protocol, we use matched backbone and training settings; non-ours results are quoted from OMP for protocol-consistent comparison.

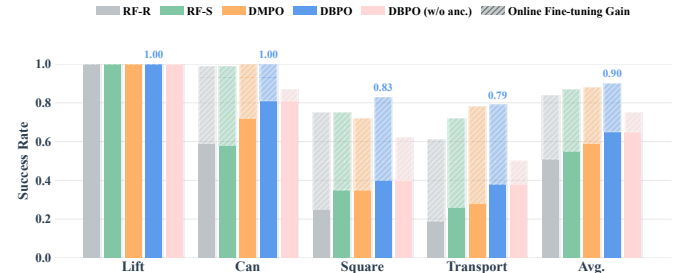
As shown in Table II, DBP achieves the best 37-task average success rate of $88.4\% \pm 3.1$, outperforming OMP (82.3%) and MP1 (78.9%) while preserving one-step deployment. In this evaluation setting, this result indicates that the proposed native one-step backbone maintains strong policy quality at scale.

The gains are broad across difficulty groups: relative to OMP, DBP improves Easy by +2.0, Medium by +12.9, Hard by +12.7, and Very Hard by +8.9. On the dexterous manipulation benchmark Adroit, DBP matches the best Hammer result, improves Door, and delivers a substantial gain on Pen (+20.0 over OMP). Compared with diffusion-style baselines in the same table (DP/DP3 at 10 NFE), DBP also attains higher overall performance under a stricter one-step inference budget. In this evaluation setting, these results support robust one-

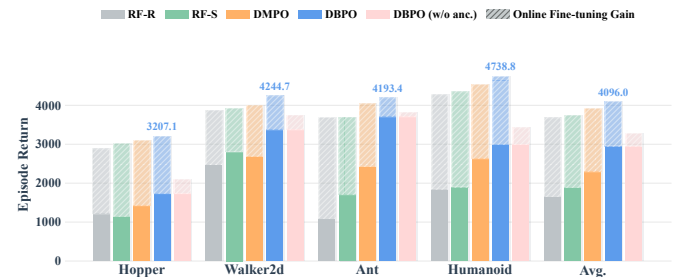
step manipulation performance and provide a stronger offline initialization for subsequent online fine-tuning.

D. Online Fine-Tuning of the DBP Backbone

We next evaluate whether PPO fine-tuning improves the pretrained drift-based one-step backbone and whether such gains transfer from sparse-reward manipulation to locomotion.



(a) RoboMimic (image-based): offline initialization and PPO fine-tuning gains.



(b) D4RL locomotion: offline initialization and PPO fine-tuning gains.

Fig. 4: Online PPO fine-tuning results on RoboMimic and D4RL with anchor ablation (DBPO vs. DBPO w/o anchor). Solid bars denote offline initialization, and hatched bars denote gains after fine-tuning. In this evaluation setting, DBPO achieves the strongest post-fine-tuning performance, while removing the anchor consistently reduces gains over pretrained baselines.

RoboMimic Policy Learning and PPO Fine-Tuning. We compare DBPO with reproduced one-step RL baselines (ReinFlow and DMPO) on sparse-reward, image-based RoboMimic tasks. Figure 4a separates offline initialization (solid bars) from fine-tuning gains (hatched bars), enabling a direct comparison of backbone quality and online adaptation effectiveness. In this evaluation setting, DBPO starts from a stronger one-step initialization and further improves after PPO fine-tuning while preserving 1-NFE deployment.

D4RL Gym Locomotion. To test cross-domain transfer, we apply the same backbone and online adapter to D4RL locomotion tasks. Figure 4b shows that DBPO attains the highest average return among compared native one-step RL baselines in this benchmark setting. In this evaluation setting, together with RoboMimic results, the trend indicates robust transfer across domains with different reward structures and action dynamics.

Anchor Ablation in Online Fine-Tuning. To validate the anchor regularizer, we evaluate a variant without it (DBPO

TABLE II: Point-cloud imitation comparison on Adroit and Meta-World under the MP1/OMP protocol. Ours refers to Drift-Based Policy. Entries report success rate (%), mean \pm std over 3 seeds). Best results are in **bold**; second-best are underlined.

Method	NFE	Adroit			Meta-World				
		Hammer	Door	Pen	Easy (21)	Medium (4)	Hard (4)	Very Hard (5)	Average
DP	10	16.0 \pm 10.0	34.0 \pm 11.0	13.0 \pm 2.0	50.7 \pm 6.1	11.0 \pm 2.5	5.25 \pm 2.5	22.0 \pm 5.0	35.2 \pm 5.3
DP3	10	100.0 \pm 0.0	56.0 \pm 5.0	46.0 \pm 10.0	87.3 \pm 2.2	44.5 \pm 8.7	32.7 \pm 7.7	39.4 \pm 9.0	68.7 \pm 4.7
Simple DP3	10	98.0 \pm 2.0	40.0 \pm 17.0	36.0 \pm 4.0	86.8 \pm 2.3	42.0 \pm 6.5	38.7 \pm 7.5	35.0 \pm 11.6	67.4 \pm 5.0
Adaflow	—	45.0 \pm 11.0	27.0 \pm 6.0	18.0 \pm 6.0	49.4 \pm 6.8	12.0 \pm 5.0	5.75 \pm 4.0	24.0 \pm 4.8	35.6 \pm 6.1
CP	1	45.0 \pm 4.0	31.0 \pm 10.0	13.0 \pm 6.0	69.3 \pm 4.2	21.2 \pm 6.0	17.5 \pm 3.9	30.0 \pm 4.9	50.1 \pm 4.7
FlowPolicy	1	98.0 \pm 1.0	61.0 \pm 2.0	54.0 \pm 4.0	84.8 \pm 2.2	58.2 \pm 7.9	40.2 \pm 4.5	52.2 \pm 5.0	71.6 \pm 3.5
MP1	1	100.0 \pm 0.0	<u>69.0</u> \pm 2.0	58.0 \pm 5.0	88.2 \pm 1.1	68.0 \pm 3.1	58.1 \pm 5.0	67.2 \pm 2.7	78.9 \pm 2.1
OMP	1	100.0 \pm 0.0	68.0 \pm 3.0	<u>60.0</u> \pm 4.0	<u>89.7</u> \pm 0.7	<u>77.4</u> \pm 2.2	<u>62.5</u> \pm 3.1	<u>77.8</u> \pm 3.0	<u>82.3</u> \pm 1.6
Ours	1	100.0 \pm 0.0	70.0 \pm 2.0	80.0 \pm 6.0	91.7 \pm 1.7	90.3 \pm 3.6	75.2 \pm 6.1	86.7 \pm 5.8	88.4 \pm 3.1

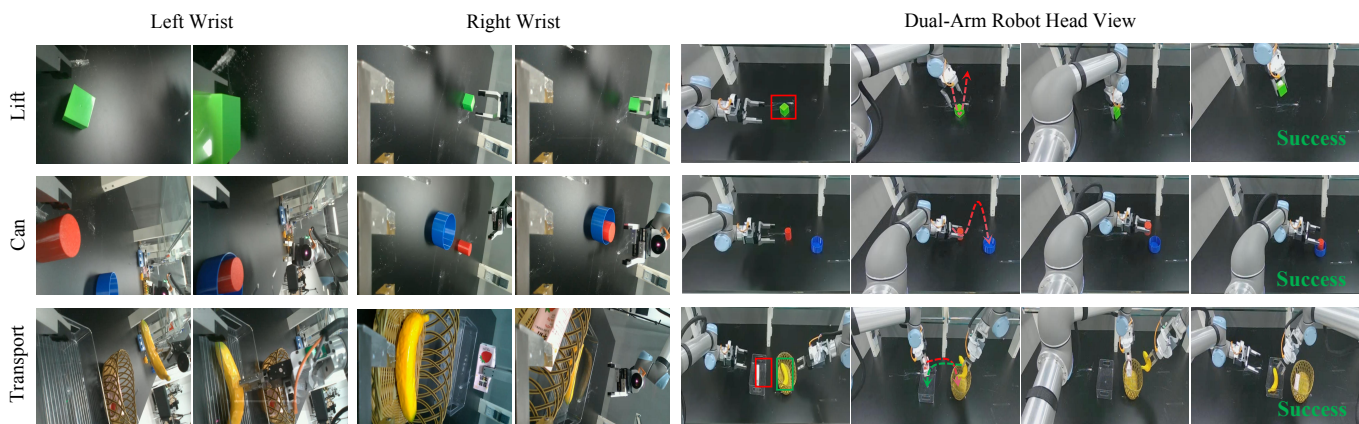


Fig. 5: Real-world bimanual deployment on the physical UR5 testbed. Drift-Based Policy executes precision Lift, Can, and synchronized bimanual Transport using raw trilateral camera inputs.

w/o anchor) on RoboMimic and D4RL. Starting from the same pretrained initialization, full DBPO achieves average scores of 0.90 on RoboMimic and 4096.0 on D4RL (Figure 4). In contrast, removing the anchor leads to performance drops to 0.75 and 3273.5, respectively. This consistent degradation confirms that the anchor is crucial for mitigating representation drift and restricting arbitrary policy deviation from the pretrained prior, thereby effectively stabilizing the online fine-tuning process.

E. Real-World Deployment

Experimental Setup and Results. To assess real-time 1-NFE feasibility, we deploy the framework on a physical dual-arm UR5 setup with an NVIDIA RTX 3090 GPU and a tri-camera array (dual wrist-mounted RealSense L515 and one Orbbec Gemini head camera). We collect 50 teleoperation demonstrations per task to train the drift-based backbone. Figure 5 shows the policy evaluated on RoboMimic-style real-world Lift, Can, and synchronized bimanual Transport tasks [42], [44].

Under severe visual occlusion and stringent hardware constraints, DBP maintains robust and reliable execution without any modification to the 1-NFE computation path. Table III clearly shows the policy consistently achieves success overall

success rate of 75.0% (45/60). The average end-to-end latency is merely 9.5 ms, strongly demonstrating the practical feasibility of one-step drifting control for high-frequency real-time robotic manipulation.

Failure Modes and System Integration. Failures stem from two recurring cases. In the Can task, grasp slip is the primary cause, where the smooth lower surface reduces contact stability, inducing sliding during lifting. Bimanual Transport failures mainly arise from inter-arm action conflicts, where one arm succeeds while the other fails to synchronize. During deployment, DBP is integrated as the high-level action generator, while the low-level dual-arm control pipeline remains unchanged. This highlights the framework’s compatibility with existing control systems, requiring no modification to the underlying hardware interface or control stack.

VI. CONCLUSION

This paper addresses a central challenge in one-step generative control, specifically achieving low-latency deployment without sacrificing policy quality. We propose Drift-Based Policy (DBP), which utilizes drift-based fixed-point training to relocate iterative refinement from inference to the training phase, thereby enabling deterministic 1-NFE action generation

TABLE III: Real-world deployment results on the physical UR5 dual-arm setup (20 trials per task).

Task	Success / Total	Success Rate (%)
Lift (Single-arm)	18 / 20	90.0%
Can (Single-arm)	16 / 20	80.0%
Transport (Bimanual)	11 / 20	55.0%
Average / Overall	45 / 60	75.0%

during deployment. We further introduce Drift-Based Policy Optimization (DBPO), a lightweight online extension that preserves the same one-step execution path while enabling exact on-policy likelihood computation for reinforcement learning. Empirical results consistently support the effectiveness of DBP and DBPO across offline imitation and online fine-tuning scenarios. Notably, DBP improves performance from 79% to 83% on the Diffusion Policy simulation suite while reducing inference cost from 100 NFE to 1 NFE. On 37 point-cloud manipulation tasks, DBP reaches an 88.4% average success rate, surpassing the prior leading 1-NFE baseline of 82.3%. DBPO further achieves competitive results on RoboMimic and D4RL benchmarks. In real-world deployment, the dual-arm UR5 setup reaches a 75% success rate at 105.2,Hz, indicating practical feasibility for high-frequency control. While current evaluations primarily target tabletop manipulation and locomotion within structured scenes, future work will extend this framework to contact-rich, long-horizon compositional tasks in less structured environments and improve DBPO sample efficiency under learning-from-scratch settings and larger model scales.

REFERENCES

- [1] C. Chi, S. Feng, Y. Du, Z. Xu, E. Cousineau, B. C. Burchfiel, and S. Song, "Diffusion Policy: Visuomotor Policy Learning via Action Diffusion," in *RSS*, 2023.
- [2] Y. Ze, G. Zhang, K. Zhang, C. Hu, M. Wang, and H. Xu, "3d diffusion policy: Generalizable visuomotor policy learning via simple 3d representations," in *RSS*, 2024.
- [3] A. Z. Ren, J. Lidard, L. L. Ankile, A. Simeonov, P. Agrawal, A. Majumdar, B. Burchfiel, H. Dai, and M. Simchowitz, "Diffusion policy optimization," in *ICLR*, 2025.
- [4] T. Zhang, C. Yu, S. Su, and Y. Wang, "Reinflow: Fine-tuning flow matching policy with online reinforcement learning," in *NeurIPS*, 2025.
- [5] G. Zou, H. Wang, H. Wu, Y. Qian, Y. Wang, and W. Li, "One step is enough: Dispersive meanflow policy optimization," *arXiv preprint arXiv:2601.20701*, 2026.
- [6] A. Prasad, K. Lin, J. Wu, L. Zhou, and J. Bohg, "Consistency policy: Accelerated visuomotor policies via consistency distillation," in *RSS*, 2024.
- [7] Z. Wang, M. Li, A. Mandlekar, Z. Xu, J. Fan, Y. Narang, L. Fan, Y. Zhu, Y. Balaji, M. Zhou, M.-Y. Liu, and Y. Zeng, "One-step diffusion policy: Fast visuomotor policies via diffusion distillation," in *ICML*, 2025.
- [8] A. Prasad, K. Lin, J. Wu, L. Zhou, and J. Bohg, "Consistency policy: Accelerated visuomotor policies via consistency distillation," in *Robotics: Science and Systems (RSS)*, 2024.
- [9] A. Clemente *et al.*, "Two-steps diffusion policy for robotic manipulation via genetic denoising," in *Advances in Neural Information Processing Systems (NeurIPS)*, 2025.
- [10] Z. Wang *et al.*, "One-step diffusion policy: Fast visuomotor policies via diffusion distillation," *arXiv preprint arXiv:2410.21257*, 2024.
- [11] J. Sheng, Z. Wang, P. Li, Y. Liu, and M. Liu, "Mpl1: Meanflow tames policy learning in 1-step for robotic manipulation," *arXiv preprint arXiv:2507.10543*, 2025.
- [12] G. Zou, H. Wang, H. Wu, Y. Qian, Y. Wang, and W. Li, "Dm1: Meanflow with dispersive regularization for 1-step robotic manipulation," *arXiv preprint arXiv:2510.07865*, 2025.
- [13] G. Zhan, L. Tao, P. Wang, Y. Wang, Y. Li, Y. Chen, H. Li, M. Tomizuka, and S. E. Li, "Mean flow policy with instantaneous velocity constraint for one-step action generation," *arXiv preprint arXiv:2602.13810*, 2026.
- [14] Z. Geng, M. Deng, X. Bai, J. Z. Kolter, and K. He, "Mean flows for one-step generative modeling," *arXiv preprint arXiv:2505.13447*, 2025.
- [15] M. Deng, H. Li, T. Li, Y. Du, and K. He, "Generative modeling via drifting," *arXiv preprint arXiv:2602.04770*, 2026.
- [16] T. Salimans and J. Ho, "Progressive distillation for fast sampling of diffusion models," *arXiv preprint arXiv:2202.00512*, 2022.
- [17] K. Frans, D. Hafner, S. Levine, and P. Abbeel, "One step diffusion via shortcut models," *arXiv preprint arXiv:2410.12557*, 2024.
- [18] Z. Wang, Z. Li, A. Mandlekar, Z. Xu, J. Fan, Y. Narang, L. Fan, Y. Zhu, Y. Balaji, M. Zhou, M.-Y. Liu, and Y. Zeng, "One-step diffusion policy: Fast visuomotor policies via diffusion distillation," *arXiv preprint arXiv:2410.21257*, 2024.
- [19] Y. Song and P. Dhariwal, "Improved techniques for training consistency models," *arXiv preprint arXiv:2310.14189*, 2023.
- [20] Y. Lipman, R. T. Q. Chen, H. Ben-Hamu, M. Nickel, and M. Le, "Flow matching for generative modeling," in *ICLR*, 2023.
- [21] Y. Song, P. Dhariwal, M. Chen, and I. Sutskever, "Consistency models," *arXiv preprint arXiv:2303.01469*, 2023.
- [22] Z. Geng, M. Deng, X. Bai, J. Z. Kolter, and K. He, "Mean flows for one-step generative modeling," in *NeurIPS*, 2025.
- [23] N. Ma, M. Goldstein, M. S. Albergo, N. M. Boffi, E. Vanden-Eijnden, and S. Xie, "Sit: Exploring flow and diffusion-based generative models with scalable interpolant transformers," in *European Conference on Computer Vision*. Springer, 2024, pp. 23–40.
- [24] P. Esser, S. Kulal, A. Blattmann, R. Entezari, J. Müller, H. Saini, Y. Levi, D. Lorenz, A. Sauer, F. Boesel, D. Podell, T. Dockhorn, Z. English, K. Lacey, A. Goodwin, Y. Marek, and R. Rombach, "Scaling rectified flow transformers for high-resolution image synthesis," 2024. [Online]. Available: <https://arxiv.org/abs/2403.03206>
- [25] X. Liu, C. Gong, and Q. Liu, "Flow straight and fast: Learning to generate and transfer data with rectified flow," in *International Conference on Learning Representations (ICLR)*, 2023.
- [26] Q. Zhang, Z. Liu, H. Fan, G. Liu, B. Zeng, and S. Liu, "Flowpolicy: Enabling fast and robust 3d flow-based policy via consistency flow matching for robot manipulation," in *Proceedings of the AAAI Conference on Artificial Intelligence (AAAI)*, 2025.
- [27] X. Hu, Q. Liu, X. Liu, and B. Liu, "Adaflow: Imitation learning with variance-adaptive flow-based policies," in *NeurIPS*, 2024.
- [28] G. Yan, J. Zhu, Y. Deng, S. Yang, R.-Z. Qiu, X. Cheng, M. Memmel, R. Krishna, A. Goyal, X. Wang, and D. Fox, "Maniflow: A general robot manipulation policy via consistency flow training," in *CoRL*, 2025.
- [29] Q. Zhang, Z. Liu, H. Fan, G. Liu, B. Zeng, and S. Liu, "FlowPolicy: Enabling fast and robust 3D flow-based policy via consistency flow matching for robot manipulation," *arXiv preprint arXiv:2412.04987*, 2024.
- [30] X. Yan *et al.*, "Maniflow: A general robot manipulation policy via consistency flow training," in *Conference on Robot Learning (CoRL)*, 2025.
- [31] H. Fang, Y. Huang, Y. Zhao, P. Weng, X. Li, and Y. Ban, "Omp: One-step meanflow policy with directional alignment," *arXiv preprint arXiv:2512.19347*, 2025.
- [32] Z. Geng *et al.*, "Improved mean flows on the challenges of fast-forward generative models," *arXiv preprint arXiv:2512.02012*, 2025.
- [33] X. Guo *et al.*, "Splitmeanflow: Interval splitting consistency in few-step generative modeling," *arXiv preprint arXiv:2507.16884*, 2025.
- [34] R. Wang and K. He, "Diffuse and disperse: Image generation with representation regularization," *arXiv preprint arXiv:2506.09027*, 2025.
- [35] G. Zou, J. Lyu, X. Li, and Z. Lu, "D2ppo: Diffusion policy optimization with dispersive loss," in *Proceedings of the AAAI Conference on Artificial Intelligence (AAAI)*, 2026.
- [36] J. Liu, G. Liu, J. Liang, Y. Li, J. Liu, X. Wang, P. Wan, D. Zhang, and W. Ouyang, "Flow-grpo: Training flow matching models via online rl," in *Advances in Neural Information Processing Systems (NeurIPS)*, 2025.
- [37] D. McAllister, S. Ge, B. Yi, C. M. Kim, E. Weber, H. Choi, H. Feng, and A. Kanazawa, "Flow matching policy gradients," *arXiv preprint arXiv:2507.21053*, 2025.
- [38] G. Lu, W. Guo, C. Zhang, Y. Zhou, H. Jiang, Z. Gao, Y. Tang, and Z. Wang, "Vla-rl: Towards masterful and general robotic manipulation with scalable reinforcement learning," *arXiv preprint arXiv:2505.18719*, 2025.

- [39] J. Schulman, F. Wolski, P. Dhariwal, A. Radford, and O. Klimov, “Proximal policy optimization algorithms,” *arXiv preprint arXiv:1707.06347*, 2017.
- [40] A. Rajeswaran, V. Kumar, A. Gupta, G. Vezzani, J. Schulman, E. Todorov, and S. Levine, “Learning complex dexterous manipulation with deep reinforcement learning and demonstrations,” in *RSS*, 2018.
- [41] R. McLean, E. Chatzaroulas, L. McCutcheon, F. Roder, T. Yu, Z. He, K. R. Zentner, R. Julian, J. K. Terry, I. Woungang, N. Farsad, and P. S. Castro, “Meta-world+: An improved, standardized, rl benchmark,” in *NeurIPS*, 2025.
- [42] A. Mandlekar, D. Xu, J. Wong, S. Nasiriany, C. Wang, R. Kulkarni, L. Fei-Fei, S. Savarese, Y. Zhu, and R. Martin-Martin, “What matters in learning from offline human demonstrations for robot manipulation,” in *CoRL*, 2021.
- [43] J. Fu, A. Kumar, O. Nachum, G. Tucker, and S. Levine, “D4rl: Datasets for deep data-driven reinforcement learning,” *arXiv preprint arXiv:2004.07219*, 2020.
- [44] T. Z. Zhao, V. Kumar, S. Levine, and C. Finn, “Learning fine-grained bimanual manipulation with low-cost hardware,” *arXiv preprint arXiv:2304.13705*, 2023.